Pramana – J. Phys. (2017) 89:69
DOI 10.1007/s12043-017-1470-4

Rope coiling

SITICHOKE AMNUANPOL

Physics Department, Thammasat University, Khlong Luang, Pathumthani 12120, Thailand
E-mail: sitichok@tu.ac.th

MS received 5 August 2016; revised 2 April 2017; accepted 1 June 2017; published online 19 October 2017

Abstract. We present the results of the combined experimental and theoretical investigation of rope coiling arising from the buckling instability. The shape of the rope is perfectly circular in the coiling region and is straight in the region below the feeding point. In between these two distant regions, the rope assumes a catenary-like shape in the limit of slow feeding velocity and a helix-like shape in the limit of fast feeding velocity. When there is an increase in the feeding velocity, the transverse displacement of deformation persists over the long distance far beyond the coiling region. The catenary is associated with the purely imaginary wave number and the helix is associated with the real wave number. The catenary-to-helix shape transition is particularly evident when the rope is fed from a large height.

Keywords. Rope; bending; twisting; buckling instability; Froude number.

PACS Nos 46.32.+x; 46.70.Hg; 61.43.−j

1. Introduction

Elastic rods arise in many contexts as the prototypical model for DNA [1], polymer [2], and cilia [3]. The characteristic, that these seemingly different materials have in common, is the ability to deform continuously in response to the forces and the moments. Typically, the minimum energy configuration of the elastic rod is a straight line. The deformation divides naturally into compression, bending, and twisting, all of which can occur simultaneously. For an elastic rod, the diameter of which is much smaller than the length, the twisting about the axis of the rod is energetically expensive, thus compression and bending are favoured. The elastic rod, subjected to the axial compression, bends laterally away from its axis. As long as the magnitude of the axial compression is above a threshold value, the transverse displacement is very large and the straight shape ceases to be stable (the buckling instability). For macroscopic systems, the buckling instability is mechanistically induced. Alternatively, the buckling instability can be intrinsically caused by an incompatibility between the geometry of the fold and the stretching of the sheet. An annular circular strip stays as planar. Folding along the centre line of the strip, which creates a crease, buckles the planar shape out of the plane to form a saddle even when no external forces are applied [4].

Previously, the rope has been used for studying knot formation. The rope plays the role of ring polymer whose rheological properties are affected by the knots [5]. After confining the rope inside a cubic box, the rotation of the cubic box entangles the rope to form several types of knots, each of which is classified by a Jones polynomial [6]. The two-dimensional version of this experiment is achieved by substituting a thin circular cell for a cubic box. So the deformation of the rope is restricted to a plane. Under the rotation of a cell the configurations of the rope are characterized in terms of the radius of gyration [7]. These preceding elegant experiments with simple apparatus inspire us to similarly exploit the ordinary rope as a representative of the elastic rod for studying buckling instability.

In our experiments, the rope is fed continuously with constant velocity from the height toward the floor. Its lower part which first makes contact with the floor is halted, while its upper part keeps moving down to the floor, compressing its lower part axially which thus bends appreciably with large transverse displacement. As a result, buckling instability occurs which gives rise to circular coiling of its lower part on the floor. By the same underlying principles, the tip of a plant root coils as it penetrates deep into the layers of the stiff soil [8]. In rope coiling the centre of the circle is static. However, it evolves in time as seen in the curling of elastic

object on a surface [9]. If an elastic thin sheet is fed instead of the rope, it folds repeatedly onto itself upon touching the floor which is the two-dimensional analog of the rope coiling. The folding of thin sheet on the floor develops a two-lobed peanut shape [10]. For a thin sheet, the large compression is relieved via a two-stage mechanism. First the sheet develops wrinkles which breaks the axial symmetry of the shape [11]. As the wrinkling grows larger, the sheet later becomes crumpled which breaks the rotational symmetry of the stress field [12]. Buckling instability is not restricted to solid-like materials. If the highly viscous liquid, such as silicone oil, is poured from a sufficient height toward the floor, the liquid filament laid out on the floor coils steadily. This phenomenon is similar to the rope coiling and is called 'liquid rope coiling' [13]. Both rope coiling and liquid rope coiling are different facets of the same buckling instability.

In §2 we describe in detail our experimental set-up for studying rope coiling. The rope has much smaller diameter than the length, a good approximation of the elastic rod. After controlling the feeding velocity and height precisely, we measure both the coiling radius and the coiling frequency. A set-up similar to ours by replacing the flat plane by the cylindrical cavity has been used for studying the compaction of elastic rod, mimicking the packing of long DNA in viral capsids [14]. We present in §3 the coiling radius and the coiling frequency along with the comparison to the experimental results reported in ref. [15]. Moreover, our results are analysed to validate the logarithmic dependence of coiling radius on the height, a prediction from the discrete elastic rods (DER) method [16]. The feeding velocity dependence of coiling radius is compared with the theoretical results obtained by a numerical continuation scheme [17]. To reveal all the possible shapes of rope coiling, we derive the equations of motion, in the approximation of small deformation, based on the balance of forces and moments. The approximation of small deformation, in which the local orientation of the rope elements changes slowly along the arc length, considerably simplifies the mathematical complication though without losing the physical essence. The values of the coefficients in these equations of motion are computed by using our experimental data of the feeding velocity and the coiling frequency. Finally, in §4 we summarize our main findings and discuss the variants of the present experiments, for instance the coiling on a moving plane.

2. Experiment

Geometrically, the rope whose radius $a_0 = 0.1$ cm has the circular cross-section area $A = 3.14 \times 10^{-2}$ cm^2 and moment of inertia of the cross-section $I = A^2/2\pi = 1.57 \times 10^{-4}$ cm^4. Its density $\rho = 0.51$ g/cm^3 and its Young's modulus $E = 2.43$ MPa. The moment of inertia of the cross-section I is a geometrical property, while the density ρ and the Young's modulus E are material properties. As sketched in figure 1, the long rope is fed from the height h to the plane below through a cylinder, whose radius is 6.4 cm, rotated by a DC motor. The frequency of rotation of the cylinder is measured by an encoder. The feeding velocity v is adjusted by tuning the voltage applied to the DC motor. The coiling frequency f is measured by a laser photoelectric sensor. The laser beam is interrupted twice for each turn of coiling. Monitoring the sensor output signals on an oscilloscope, we can read off the period of coiling whose inverse is f.

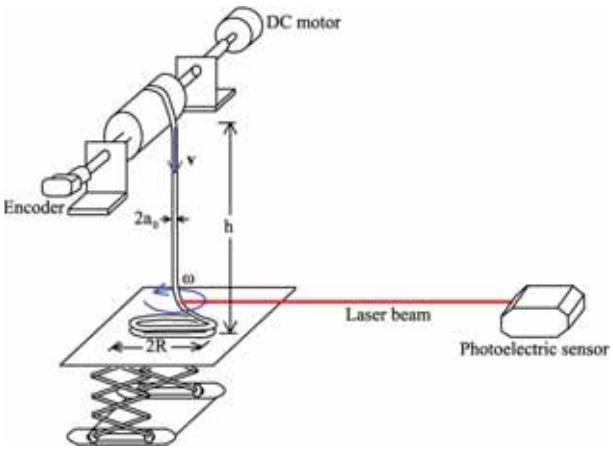

Figure 1. Experimental set-up is shown schematically. The rope with diameter $2a_0$ is fed with uniform velocity v from the height h to the plane. It is laid down on the plane in a circular shape with the diameter $2R$ and the angular velocity $\omega = 2\pi f$. The feeding velocity v is calculated from the radius of the cylinder and the frequency of the cylinder rotation measured by an encoder. The coiling frequency f is measured by a laser photoelectric sensor.

The rope is so soft and slender that its own weight is sufficient for the buckling instability irrespective of what the height h is. One end of the rope that reaches the plane is fixed, whereas the other end of the rope at feeding point above is free. For such boundary conditions the critical force of the rope with length L is $F_c = (\pi^2/4)EI/L^2$, above which buckling instability occurs [19]. Generally, $2R$, the diameter of coiling, is much smaller than the height h. Hence the length L is reasonably approximated by the height h, roughly speaking $F_c \approx (\pi^2/4)EI/h^2$. It is difficult to buckle the rope fed from small height h because larger force is required to overcome F_c. Considering the most difficult buckled situation, i.e. the minimum height $h = 10.5$ cm, the critical force $F_c = 8.53 \times 10^{-4}$ N. The rope with the

length equal to the height h has the mass $\rho Ah = 0.17$ g corresponding to the weight 1.7×10^{-3} N which is still larger than F_c. The rope's own weight alone is already sufficient for buckling instability.

3. Results and discussion

We emphasize how the coiling radius R and the coiling frequency f depend on the height h and the feeding velocity v. Our results are compared with the experiments [15], the DER simulations [16], and the numerical solutions of the Kirchhoff–Love equations by the continuation method [17]. Next, we turn our attention to the shape of the rope during coiling. The coiling portion on a plane is perfectly circular whereas the top portion near the feeding point is straight. The interesting question is the shape assumed by the rope between these two separated portions. The solutions of the equations of motion suggest that the rope shape varies from a catenary to a helix as v increases.

3.1 *Coiling radius and coiling frequency*

The forces playing a primary role in rope coiling are the elastic force, gravitational force, and inertial force. Let F_E is the elastic force per unit length, F_G is the gravitational force per unit length, and F_I is the inertial force per unit length whose expressions are respectively [15]

$$F_E \approx \frac{E(2a_0)^4}{R^3}, \quad F_G \approx \rho g(2a_0)^2,$$
$$F_I \approx \frac{\rho(2a_0)^2 v^2}{R}. \tag{1}$$

The interplay of these three forces determines the regimes of the rope coiling that could be elastic, gravitational, or inertial depending on which force is dominant.

When the rope is fed slowly from the small height, the elastic force dominates the gravitational and inertial forces, so-called the elastic coiling. The net force acting on any element of the rope is zero. The coiling radius $R \sim h$ increases with the height h as shown in figure 2a. The conservation of the rope mass requires $v = 2\pi f R$, thus the coiling frequency $f = v/2\pi R \sim v/h$ decreases inversely with increasing h in qualitative agreement with figure 2b. The fact that the coiling radius R increases with height h and that the coiling frequency f correspondingly decreases with height h is to keep the feeding velocity v constant. Interestingly, the Young's modulus E and the density ρ do not appear in the expressions of the coiling radius R and of the coiling frequency f. In elastic coiling the coiling radius R and coiling frequency f are independent of the material making up the rope.

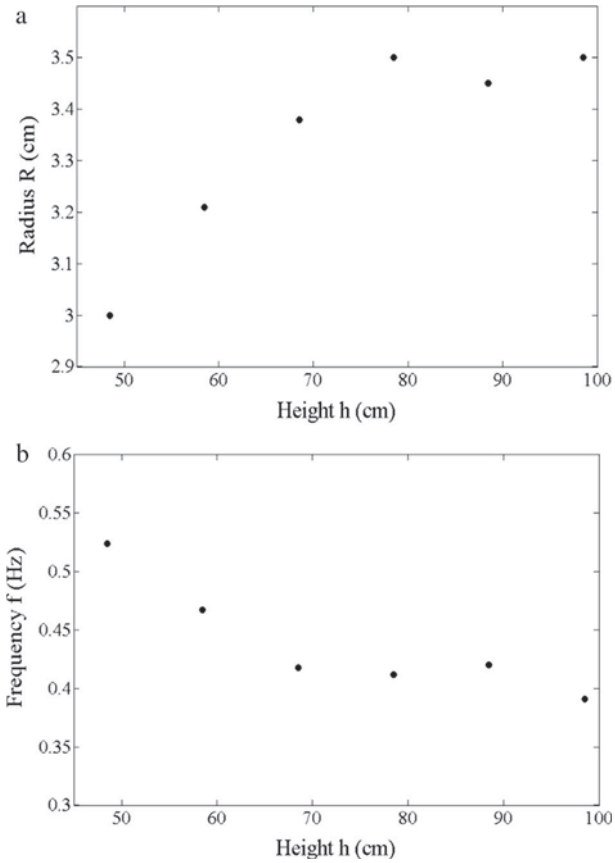

Figure 2. Behaviour in the elastic coiling. (**a**) When the height varies from 48.5 to 98.5 cm, the rope fed with sufficiently slow feeding velocity $v = 9$ cm/s from the larger height h coils with the larger radius R. (**b**) For the same range of h and v, the rope fed from the larger height h coils with the slower frequency f.

For the rope fed slowly from the large height, the elastic force is balanced by the gravitational force, $F_E = F_G$, determining the radius $R = (E(2a_0)^2/\rho g)^{1/3} \approx 12.5$ cm for our experiments. To fall into the regime of gravitational coiling, the height h should be much larger than 12.5 cm. The coiling frequency, computed via $f = v/2\pi R$, is thus $f = (v/2\pi)(\rho g/E(2a_0)^2)^{1/3}$ increasing linearly with the feeding velocity v. In contrast to elastic coiling, the coiling frequency f in gravitational coiling is height independent as illustrated in figure 3a. To ensure the gravitational force dominating over the inertial force, the feeding velocity v is kept sufficiently slow and the height h is large. At $h = 168.5$ cm shown in figure 3b, the coiling frequency f increases to some extent linearly with v in the range from 3 to 11 cm/s beyond which it starts to level off.

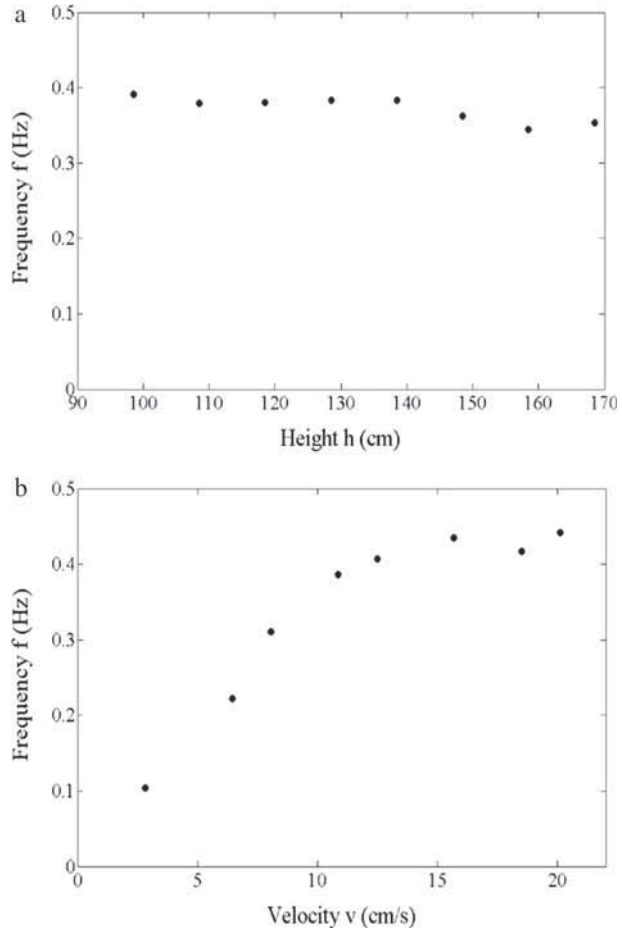

Figure 3. Behaviour in the gravitational coiling. (**a**) The coiling frequency f is relatively independent of height h when the height varies from 98.5 to 168.5 cm with the sufficiently slow feeding velocity $v = 9$ cm/s. (**b**) At height 168.5 cm, the coiling frequency f increases rather linearly with the feeding velocity v in the slow feeding velocity range from 3 to 11 cm/s.

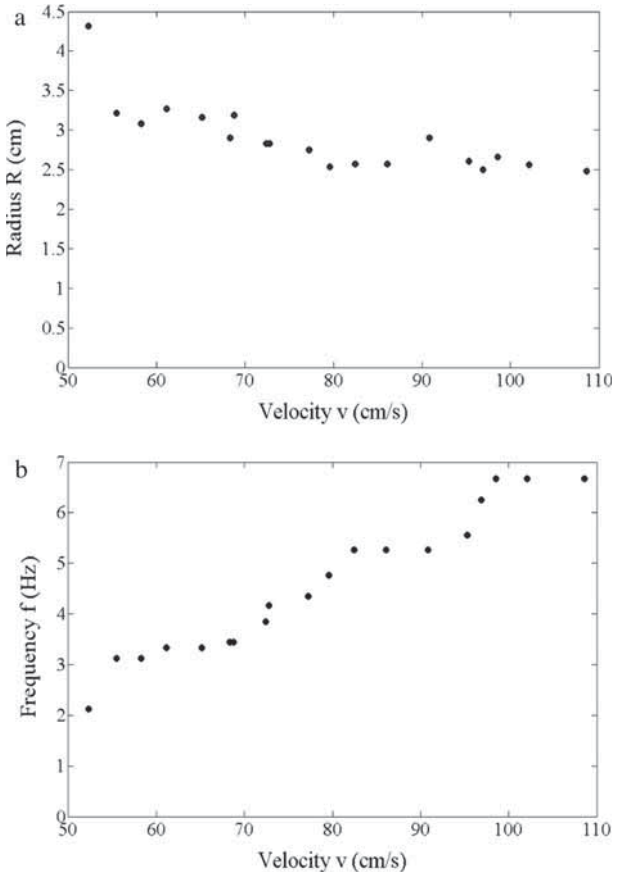

Figure 4. Behaviour in the inertial coiling. (**a**) At 28.5 cm height the coiling radius R gets smaller as rope is fed to the plane with the faster feeding velocity v. (**b**) At the same height the coiling frequency f increases with v faster than it does in the gravitational coiling.

For the rope fed rapidly from the small height, the elastic force is now balanced by the inertial force, $F_E = F_I$, determining the coiling radius $R = (2a_0/v)\sqrt{E/\rho}$ which is qualitatively consistent with the feeding velocity dependence of the coiling radius shown in figure 4a. The coiling frequency, computed via $f = v/2\pi R$, is $f = (v^2/4\pi a_0)\sqrt{\rho/E}$ increasing quadratically with the feeding velocity v unlike the linear v dependence of f observed in gravitational coiling. The dominance of inertial force calls for the fast feeding velocity v and the small height h. At $h = 28.5$ cm and the range of v from 52 to 109 cm/s, shown in figure 4b, the overall trend of the coiling frequency f increases with v faster than linearly. The fastest feeding velocity of 109 cm/s is still far below the velocity of the propagation of elastic waves, for example sound waves propagating in the rope with velocity $\sqrt{E/\rho} \approx 6900$ cm/s.

Our results, figures 2, 3 and 4, are insensitive to the friction force between the rope and the plane, because no significant changes in the coiling radius R and coiling frequency f are observed when changing the material making up the plane. Furthermore, R and f are measured after a few initial coiling turns to minimize the transient effects possibly caused by the small deviation of position of the point of contact. The unimportance of friction force relative to the axial compressive forces, i.e. gravitational force and inertial force, is consistent with the fact that the buckling instability is the onset of deformation by bending in response to the axial compressive forces not in response to the shear forces, such as friction force whose direction is off the axis of rope.

The feeding velocity dependence of coiling radius R, shown in figure 5a for the entire range of feeding velocities encompassing all three regimes, agrees qualitatively with figure 2 in ref. [15]. Given a height h the coiling radius R initially increases with increasing feeding velocity v, and reaches a maximum about

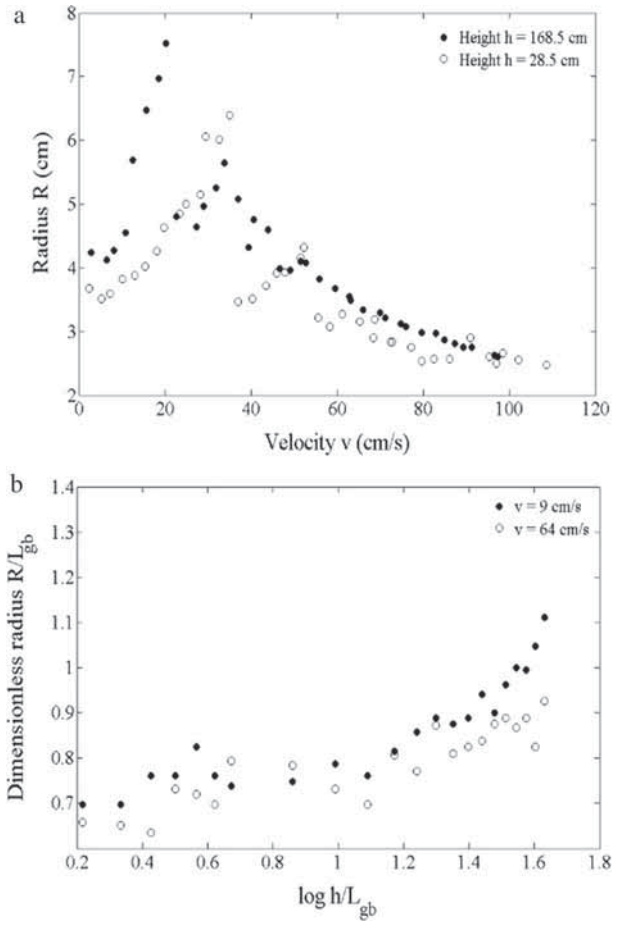

Figure 5. Coiling radius over the entire range of feeding velocity and height. (**a**) There exists a characteristic velocity at which coiling radius R is the largest. Above this characteristic velocity, the inertial force is dominant. The peak of R is a signature of the entry to the inertial coiling regime. (**b**) Scaling both the coiling radius R and the height h by the gravito-bending length $L_{\rm gb} = (Ea_0^2/8\rho g)^{1/3} = 3.9\,$cm in our experiments, the linear fit to $R/L_{\rm gb}$ versus $\log\ h/L_{\rm gb}$ graph gives the slopes 0.22 for $v = 9$ cm/s and 0.16 for $v = 64$ cm/s both of which are in good agreement with the value 0.27 reported in ref. [16] using the DER simulations.

$v \approx 20$ cm/s for $h = 168.5$ cm and about $v \approx 35$ cm/s for $h = 28.5$ cm. Above these feeding velocities, it turns out that R decreases with increasing v. A dramatic change in behaviour of R, as v passes across the value at which R is maximum, signifies a cross-over of elastic coiling and inertial coiling. The numerical study by the DER method reveals the logarithmic dependence of the dimensionless coiling radius on the dimensionless height, that is $R/L_{\rm gb} = 0.27\log(h/L_{\rm gb}) + 1.27$ where $L_{\rm gb} = (Ea_0^2/8\rho g)^{1/3}$ denotes the gravito-bending length [16]. Plotting $R/L_{\rm gb}$ vs. $\log(h/L_{\rm gb})$ as shown in figure 5b, the linear fit to our data yields slope 0.22 and intercept 0.62 for $v = 9$ cm/s, and slope 0.16 and intercept 0.61 for $v = 64$ cm/s. The slopes depend weakly

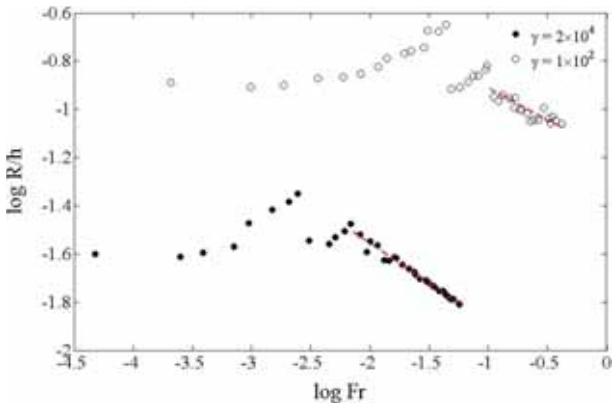

Figure 6. To compare with the theoretical results, figure 2a in ref. [17], we scale the coiling radius R by the height h. The feeding velocity v is quantified in terms of the Froude number $\mathrm{Fr} \sim v^2/gh$ and the height h is quantified in terms of the dimensionless parameter $\gamma \sim \rho A g h^3/EI$. The parameter $\gamma = 2 \times 10^4$ corresponds to $h = 168.5$ cm and $\gamma = 1 \times 10^2$ corresponds to $h = 28.5$ cm. In both cases of γ, $\log\ R/h$ has a linear relation with $\log$ Fr when Fr grows large enough. The dashed lines, which are the linear fit to the data in the range of large Fr, have the slopes -0.33 for $\gamma = 2 \times 10^4$ and -0.26 for $\gamma = 1 \times 10^2$ both of which are the same magnitude order as the theoretically predicted one $-1/2$.

on v and agree well with the value 0.27 obtained from the DER method.

To make a contact with the theory we plot, on the log–log scale, the dimensionless coiling radius R/h vs. the Froude number $\mathrm{Fr} \sim v^2/gh$ which is the ratio of the kinetic energy $\rho A h v^2/2$ to the gravitational energy $\rho A g h^2$. Let $\gamma \sim \rho A g h^3/EI$ be the ratio of the gravitational energy to the flexural energy EI/h. In figure 6 given a height 168.5 cm, i.e. $\gamma = 2 \times 10^4$ for the filled circle data points, increasing the Froude number Fr by feeding the rope more rapidly with larger v, the dimensionless coiling radius R/h first remains relatively constant and then rises once Fr reaches about 10^{-3}. However, further increase in Fr above $10^{-2.5}$ turns out to make the dimensionless coiling radius smaller. At a small height of 28.5 cm, i.e. $\gamma = 1 \times 10^2$ for the opened circle data points, the dimensionless coiling radius R/h shows the same dependence on Fr except for the fact that Fr, above which R/h decreases with increasing Fr, is shifted to $10^{-1.5}$ higher than $10^{-2.5}$ for $\gamma = 2 \times 10^4$. The graphs are relatively linear when $\mathrm{Fr} > 10^{-2}$ for $\gamma = 2 \times 10^4$, and when $\mathrm{Fr} > 10^{-1}$ for $\gamma = 1 \times 10^2$. This linear dependence can be understood by recalling the coiling radius $R = (2a_0/v)\sqrt{E/\rho}$ in the inertial coiling regime, which can be casted in terms of Fr and γ as $R/h \sim \mathrm{Fr}^{-1/2}\gamma^{-1/2}$. As a result, the theoretically predicted slope is $-1/2$ on the log–log scale, which agrees well with the slopes obtained from the linear fit to the

data shown as the dashed lines. Such a linear relation between $\log R/h$ and $\log \mathrm{Fr}$ marks the onset of inertial coiling regime.

Our experimental results, figure 6, shows that the general features are in good agreement with figure 2a in ref. [17] obtained from solving numerically the Kirchhoff–Love equations by the scheme of the continuation method. Although we cannot observe the theoretically predicted behaviour, $R/h \sim \mathrm{Fr}^{1/3}$, for $\mathrm{Fr} > 10$. In realistic experimental situations, the rope fed with the a fast feeding velocity v coils up noncircularly, because the collision with the plane generates such a strong force on the rope that its coiling is largely distorted to a disordered shape. Hence the coiling radius R now becomes ill-defined. The coiling shape becomes disordered before we reach the $\mathrm{Fr} > 10$ range. We must stop at $v = 97$ cm/s for 168.5 cm height and at $v = 109$ cm/s for 28.5 cm height. Above these two velocities, the coiling is no longer circular.

3.2 *Shape in the region between coiling portion and feeding point*

In the absence of external forces and external moments, the straight line with zero curvature and zero torsion is the minimum energy configuration. The shape deviation from the straight line is a response of elastic rope to the gravitational force and inertial force. Such a deviation is largest in the coiling region on the plane and is zero in the vicinity of the feeding point. The shape in the coiling region is definitely circular. However, the shape in the region between the coiling portion and the feeding point exhibits a variety of forms ranging from a catenary in the gravitational-force dominated regime to a helix in the inertial-force dominated regime [17]. The displacement consists of the longitudinal component, parallel to the axis of the rope, and the transverse component, perpendicular to the axis of the rope. The coiling radius R is set by the largest magnitude of transverse component.

Let $\mathbf{r}(s,t)$ be the position vector of the point on the rope at arc length s and at instant time t. Without losing the generality we choose the xy-plane to be the plane in which rope coiling takes place, and the z-axis to be the vertical axis perpendicular to this plane that passes through the centre of the coiling circle assumed to be the origin $(0,0,0)$. One end of the rope at the point of contact on the xy-plane is assigned the arc length $s = 0$ and the other end at the feeding point is assigned $s = L$. $\mathbf{F}$ is the the resultant internal stress. Balancing the forces gives the equations of motion [18]

$$\frac{\partial \mathbf{F}}{\partial s} + \rho A\mathbf{g} = \rho A \frac{\partial^2 \mathbf{r}}{\partial t^2}, \tag{2}$$

where gravitational acceleration $\mathbf{g} = -g\hat{\mathbf{z}}$. The element at arc length s has the velocity whose magnitude equals the feeding velocity v and whose direction is along the tangent vector $\hat{\mathbf{t}} = \partial\mathbf{r}/\partial s$. So its velocity $\mathbf{v}(s) = v\partial\mathbf{r}/\partial s$. The change in velocity contributes $v^2\partial^2\mathbf{r}/\partial s^2$ to the acceleration of this element. In the reference frame co-rotating with the rope, this element also experiences the acceleration due to the Coriolis force, $2\boldsymbol{\omega}\times\mathbf{v}$, and the acceleration due to the centrifugal force, $\boldsymbol{\omega}\times(\boldsymbol{\omega}\times\mathbf{r})$. In such a rotating reference frame, we can write the acceleration

$$\frac{\partial^2 \mathbf{r}}{\partial t^2} = v^2\frac{\partial^2 \mathbf{r}}{\partial s^2} + 2v\boldsymbol{\omega}\times\frac{\partial \mathbf{r}}{\partial s} + \boldsymbol{\omega}\times(\boldsymbol{\omega}\times\mathbf{r}), \tag{3}$$

where angular velocity $\boldsymbol{\omega} = \omega\hat{\mathbf{z}}$. The advantage of analysing in a rotating frame rather than in a laboratory frame is that the rope coiling is seen steady, namely the time-independent position vector $\mathbf{r}(s)$ is a function of arc length s only. The resultant internal stress $\mathbf{F}$ varies spatially along the arc length

$$\frac{\partial \mathbf{F}}{\partial s} = -\rho A\mathbf{g} + \rho A v^2\frac{\partial^2 \mathbf{r}}{\partial s^2} + 2\rho A v\boldsymbol{\omega}\times\frac{\partial \mathbf{r}}{\partial s} + \rho A\boldsymbol{\omega}\times(\boldsymbol{\omega}\times\mathbf{r}). \tag{4}$$

Now we turn to consider the moment of the resultant internal stress denoted by $\mathbf{M}$. Balancing of moments gives the additional equations of motion which in steady coiling take a simple form

$$\frac{\partial \mathbf{M}}{\partial s} = \mathbf{F}\times\hat{\mathbf{t}}. \tag{5}$$

Bending and twisting occur simultaneously. The bending causes a local change in velocity $\mathbf{v}(s)$ which contributes to $\mathbf{M}$ the term $\partial^2\mathbf{r}/\partial s^2$, and the twisting causes a rotation of two adjacent cross-sections relative to each other by an angle τ which contributes to $\mathbf{M}$ the term proportional to τ. Adding up these two contributions from bending and twisting leads to the moment

$$\mathbf{M} = EI\frac{\partial \mathbf{r}}{\partial s}\times\frac{\partial^2 \mathbf{r}}{\partial s^2} + GJ\tau\frac{\partial \mathbf{r}}{\partial s}, \tag{6}$$

where G is the shear modulus and J is the polar moment of inertia of the cross-section. For small deformations, the orientation of the rope element varies slowly along the arc length. Differentiating eq. (5) with respect to the arc length s gives [19]

$$\frac{\partial^2 \mathbf{M}}{\partial s^2} = \frac{\partial \mathbf{F}}{\partial s}\times\hat{\mathbf{t}}. \tag{7}$$

As the term $\mathbf{F}\times \mathrm{d}\hat{\mathbf{t}}/\mathrm{d}s$ is negligibly small when $\hat{\mathbf{t}}$ varies slowly, this term does not appear in eq. (7).

An important consequence of small deformation is that the derivative with respect to the arc length s can be accurately approximated by the derivative with respect

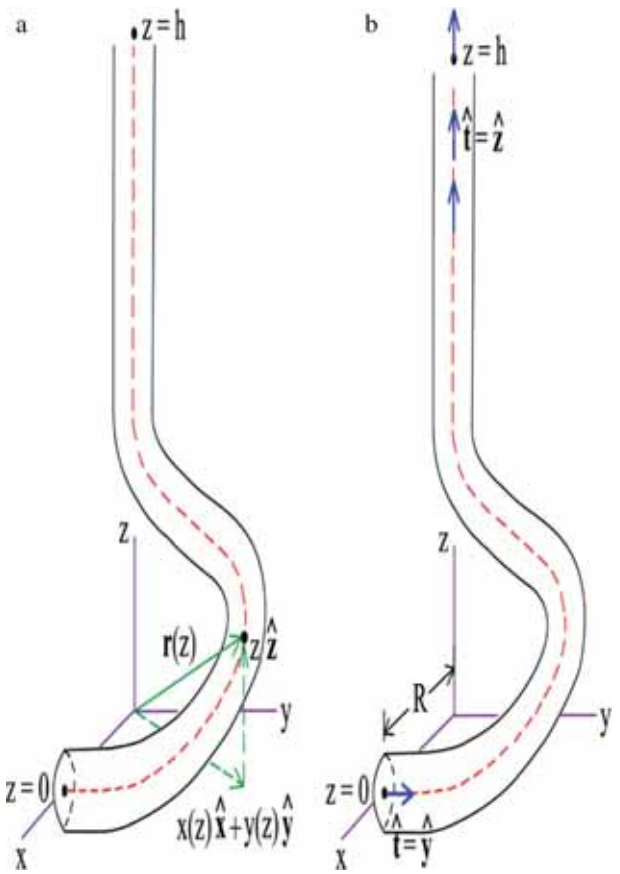

Figure 7. For small deformation the position vector $\mathbf{r}(z)$ can be parametrized by the z coordinate rather than by the arc length s. (**a**) The point of contact corresponds to $z = 0$ and the feeding point corresponds to $z = h$. The bending is clearly seen in the portion of rope just above the $z = 0$ plane. (**b**) The boundary conditions at the point of contact and at the feeding point, eqs. (9) and (10), are illustrated geometrically.

to the coordinate z. The transverse components of the displacement $x(z)$ and $y(z)$ are thus expressed as a function of the coordinate z instead of as a function of the arc length s. For small deformation, the position vector is thus written as $\mathbf{r}(z) = x(z)\hat{\mathbf{x}} + y(z)\hat{\mathbf{y}} + z\hat{\mathbf{z}}$ illustrated in figure 7a. The rope is fed from $z = h$ down to the $z = 0$ plane below. Let us choose the x-axis passing through the point of contact where the rope first touches the plane. Substituting the left- and right-hand sides of eq. (7) by eqs (6) and (4) respectively, we obtain

$$\begin{aligned}
&\frac{\mathrm{d}^4x}{\mathrm{d}z^4} + \frac{\rho A v^2}{EI}\frac{\mathrm{d}^2x}{\mathrm{d}z^2} - \frac{\rho A g}{EI}\frac{\mathrm{d}x}{\mathrm{d}z} - \frac{\rho A\omega^2}{EI}x \\
&\quad + \tau\frac{GJ}{EI}\frac{\mathrm{d}^3y}{\mathrm{d}z^3} - 2\frac{\rho A v\omega}{EI}\frac{\mathrm{d}y}{\mathrm{d}z} = 0 \\
&\frac{\mathrm{d}^4y}{\mathrm{d}z^4} + \frac{\rho A v^2}{EI}\frac{\mathrm{d}^2y}{\mathrm{d}z^2} - \frac{\rho A g}{EI}\frac{\mathrm{d}y}{\mathrm{d}z} - \frac{\rho A\omega^2}{EI}y \\
&\quad - \tau\frac{GJ}{EI}\frac{\mathrm{d}^3x}{\mathrm{d}z^3} + 2\frac{\rho A v\omega}{EI}\frac{\mathrm{d}x}{\mathrm{d}z} = 0. \qquad (8)
\end{aligned}$$

The second-derivative terms arise from the inertial force, the first-derivative terms arise from the gravitational force, and the linear terms arise from the centrifugal force. Two x and y components of transverse displacement are coupled through the twist of the rope, which gives rise to the third derivative terms, and through the Coriolis force which gives rise to the first-derivative terms. In figure 7b, the x-axis passes through the point of contact and therefore the x component at $z = 0$ equals the coiling radius, i.e., $x(0) = R$, and the y component at $z = 0$ equals zero, i.e., $y(0) = 0$. At the point of contact, the rope orientates parallel to the y-axis, that is to say $\hat{\mathbf{t}} = \hat{\mathbf{y}}$ corresponding to $\mathrm{d}x/\mathrm{d}z|_{z=0} = 0$, $\mathrm{d}y/\mathrm{d}z|_{z=0} = 1$. For small deformation, the tangent vector $\hat{\mathbf{t}}$ changes so slowly that all the higher-order derivatives vanish identically. To summarize, the boundary conditions at the point of contact are

$$\begin{aligned}
&x(0) = R, \quad \left.\frac{\mathrm{d}x}{\mathrm{d}z}\right|_{z=0} = 0, \\
&\left.\frac{\mathrm{d}^2x}{\mathrm{d}z^2}\right|_{z=0} = 0, \quad \left.\frac{\mathrm{d}^3x}{\mathrm{d}z^3}\right|_{z=0} = 0 \\
&y(0) = 0, \quad \left.\frac{\mathrm{d}y}{\mathrm{d}z}\right|_{z=0} = 1, \\
&\left.\frac{\mathrm{d}^2y}{\mathrm{d}z^2}\right|_{z=0} = 0, \quad \left.\frac{\mathrm{d}^3y}{\mathrm{d}z^3}\right|_{z=0} = 0. \qquad (9)
\end{aligned}$$

In figure 7b the feeding point is vertically above the origin by the height h, and therefore the x and y components at $z = h$ are $x(h) = 0, y(h) = 0$. In the vicinity of the feeding point, the rope orientates parallel to the z-axis, that is to say $\hat{\mathbf{t}} = \hat{\mathbf{z}}$ corresponding to $\mathrm{d}x/\mathrm{d}z|_{z=h} = 0$, $\mathrm{d}y/\mathrm{d}z|_{z=h} = 0$. Just below the feeding point, the tangent vector $\hat{\mathbf{t}}$ points along the z direction and so all the higher-order derivatives vanish identically. To summarize, the boundary conditions at the feeding point are

$$\begin{aligned}
&x(h) = 0, \quad \left.\frac{\mathrm{d}x}{\mathrm{d}z}\right|_{z=h} = 0, \\
&\left.\frac{\mathrm{d}^2x}{\mathrm{d}z^2}\right|_{z=h} = 0, \quad \left.\frac{\mathrm{d}^3x}{\mathrm{d}z^3}\right|_{z=h} = 0 \\
&y(h) = 0, \quad \left.\frac{\mathrm{d}y}{\mathrm{d}z}\right|_{z=h} = 0, \\
&\left.\frac{\mathrm{d}^2y}{\mathrm{d}z^2}\right|_{z=h} = 0, \quad \left.\frac{\mathrm{d}^3y}{\mathrm{d}z^3}\right|_{z=h} = 0. \qquad (10)
\end{aligned}$$

In the more elaborate calculation using the Kirchoff–Love equations capable of large deformation, the twist angle τ is constant over the entire length of the rope [17]. The undeformed configuration of the rope is a twistless straight line. If the twist is not injected at the feeding

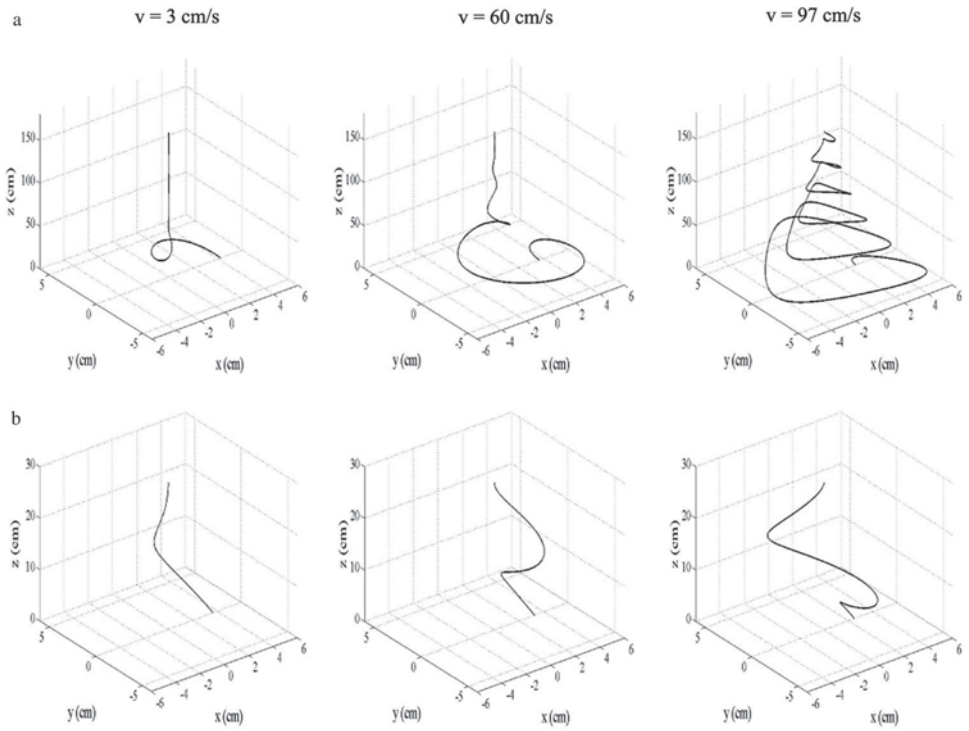

Figure 8. Shape variation with feeding velocity. (**a**) For height 168.5 cm the stronger inertial force resulted from the fast feeding velocity v creates the additional curvature particularly in the vicinity of the feeding point. Evidently, the shape is catenary-like at $v = 3$ cm/s but is helix-like at $v = 97$ cm/s. (**b**) For smaller height 28.5 cm the change in shape becomes less pronounced.

point, the rope remains twistless ($\tau = 0$) throughout coiling. With the two-point boundary conditions, eqs (9) and (10), we thus set the twist angle $\tau = 0$ in eq. (8) and rely on our experimental data of the feeding velocity v and of the coiling frequency f for evaluating the values of three coefficients $\rho A v^2/EI$, $\rho A \omega^2/EI$, and $\rho A v\omega/EI$ which appear in eq. (8). To impose the boundary conditions, we use our experimental data of the coiling radius R for eq. (9) and that of the height h for eq. (10). After solving eq. (8) numerically for the $x(z)$ and $y(z)$ components of transverse displacement, the shape of the rope can be reconstructed from the position vector $\mathbf{r}(z) = x(z)\hat{\mathbf{x}} + y(z)\hat{\mathbf{y}} + z\hat{\mathbf{z}}$.

The shape in the neighbourhood of the feeding point $z = h$ is vertically straight for the slow feeding velocity v. In figure 8a, for $h = 168.5$ cm, by increasing v the shape develops a curvature in the region near the feeding point $z = h$. This curvature induced by the inertial force persists over a distance along the z-axis. For $v = 97$ cm/s the inertial force-induced curvature extends over the long distance, thereby changing the shape to look more like a helix. The change in shape with feeding velocity v is less apparent for small height $h = 28.5$ cm (see figure 8b), because the rope with the shorter length has more resistance to buckle and tries to maintain its straight configuration. In figures 8a and 8b, the x component at the point of contact, $x(0) = R$, is not a fixed value because the experiments show that the coiling radius R is height-dependent and velocity-dependent (please see figures 2a and 4a respectively).

The transverse displacement, i.e. the x and y components of $\mathbf{r}$, is the largest at $z = 0$ and is zero at $z = h$. As we move upward from $z = 0$ to $z = h$, the transverse displacement must gradually diminish to zero. The persistence length λ_p measures the extent of the transverse displacement. The rope fed rapidly toward the plane with fast feeding velocity v is subjected to stronger inertial force, thus acquires the larger transverse displacement which persists over a long distance. This physical reasoning suggests that the fast feeding velocity v would lead to the longer persistence length λ_p. In what follows, we study more quantitatively the dependence of λ_p on the feeding velocity v and height h. The persistence length λ_p is largely determined by the elastic properties of the rope. Any physically reasonable boundary conditions at $z = 0$ and $z = h$ do not have an appreciable effect on λ_p. In thermodynamic limit, i.e., when $L \to \infty$, we can take the Fourier transformation, $x(z) = (1/2\pi)\int \mathrm{d}k \exp(ikz)x(k)$ and $y(z) = (1/2\pi)\int \mathrm{d}k \exp(ikz)y(k)$. In momentum space we can express eq. (8) in the matrix form

$$\begin{bmatrix} A_{11} & A_{12} \\ A_{21} & A_{22} \end{bmatrix} \begin{bmatrix} x(k) \\ y(k) \end{bmatrix} = \begin{bmatrix} 0 \\ 0 \end{bmatrix}, \tag{11}$$

where the matrix elements are

$$A_{11} = k^4 - \frac{\rho A v^2}{EI}k^2 - i\frac{\rho A g}{EI}k - \frac{\rho A \omega^2}{EI}$$
$$A_{12} = -i\left(\tau\frac{GJ}{EI}k^3 + 2\frac{\rho A v\omega}{EI}k\right)$$
$$A_{21} = i\left(\tau\frac{GJ}{EI}k^3 + 2\frac{\rho A v\omega}{EI}k\right)$$
$$A_{22} = A_{11}. \quad (12)$$

The existence of the nonzero $x(k)$, $y(k)$ components requires the determinant of the 2×2 matrix vanishing, resulting in two fourth-degree polynomials

$$k^4 - \tau\frac{GJ}{EI}k^3 - \frac{\rho A v^2}{EI}k^2 - \left(2\frac{\rho A v\omega}{EI} + i\frac{\rho A g}{EI}\right)k - \frac{\rho A \omega^2}{EI} = 0 \quad (13)$$

and

$$k^4 + \tau\frac{GJ}{EI}k^3 - \frac{\rho A v^2}{EI}k^2 + \left(2\frac{\rho A v\omega}{EI} - i\frac{\rho A g}{EI}\right)k - \frac{\rho A \omega^2}{EI} = 0 \quad (14)$$

whose roots are the wave numbers k. Note that the coefficients of the linear term k in eqs (13) and (14), resulted from the Coriolis force and the gravitational force, are complex numbers. Changing the wave number k to $(-k)^*$ transforms eqs (13)–(14) and vice versa, suggesting that if $k = k_{\rm re} + ik_{\rm im}$ is the root of eq. (13) then $k = -k_{\rm re} + ik_{\rm im}$ is the root of eq. (14). The fact that the transverse displacement reduces towards the feeding point $z = h$ constrains the imaginary part $k_{\rm im}$ to be positive. A fourth-degree polynomial possesses four roots of k, one of which is physically meaningful. The inverse of its imaginary part gives persistence length, namely $\lambda_{\rm p} = 1/k_{\rm im}$.

For twistless rope, i.e. $\tau = 0$, the persistence length $\lambda_{\rm p}$ gets longer when rope is fed rapidly with the fast feeding velocity v as shown in figure 9a. The different heights $h = 168.5$ and 28.5 cm seem to have a little effect on $\lambda_{\rm p}$. Notice that for 28.5 cm height the feeding velocity v of about 36 cm/s gives $\lambda_{\rm p}$ being the order of the height h. This implies that feeding the rope faster than 36 cm/s lengthens $\lambda_{\rm p}$ more than the height h itself. In other words, the appreciable transverse displacement persists even up to the region close to the feeding point $z = h$. In figure 9b the shape in the limit of infinitesimally slow feeding velocity is a catenary whose wave number k is purely imaginary. In contrast, the shape in the limit of infinitely fast feeding velocity is a helix, except from being straight just below the feeding point to satisfy the boundary conditions eq. (10), whose wave number k is real. In the range of intermediate feeding velocities, the shape is a superposition of catenary and helix, with the appropriate weights, whose wave number k has both real part and imaginary part. The catenary-to-helix transition upon increasing the feeding velocity v associates with the real part $k_{\rm re}$ larger but the imaginary part $k_{\rm im}$ smaller, the latter in turn yields the longer persistence length $\lambda_{\rm p}$.

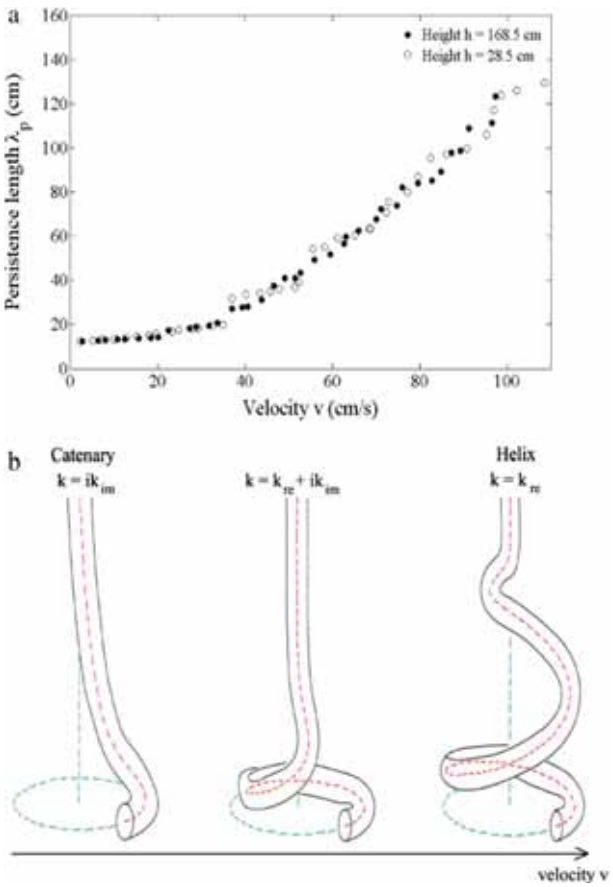

Figure 9. Persistence length $\lambda_{\rm p}$ as a function of feeding velocity v. (**a**) Persistence length $\lambda_{\rm p}$, which is the inverse of the imaginary part of the wave number root of eq. (13) or (14), increases with v for height $h = 168.5$ cm (shown by the filled circles) and for height $h = 28.5$ cm (opened circles). (**b**) This feeding velocity dependence of $\lambda_{\rm p}$ can be understood on a basis that on increasing v the shape changes from a catenary to a helix. Accordingly, the wave number root changes from being purely imaginary to being real, indicative of the fact that on increasing v the real part becomes larger whereas the imaginary part becomes smaller. The inverse of the smaller imaginary part therefore gives longer persistence length $\lambda_{\rm p}$ for the faster feeding velocity v.

4. Conclusions

Coiling is a manifestation of the buckling instability which occurs when an axial compressive force exceeds

the critical force $F_c = CEI/L^2$, where C is a constant depending on the types of the boundary conditions that could be free, clamped, or hinged. Both the coiling radius R and the coiling frequency f behave differently in three distinct regimes of elastic coiling, gravitational coiling, and inertial coiling. In liquid rope coiling the viscous force plays the role of elastic force, hence elastic coiling is replaced by viscous coiling in which the coiling frequency f decreases by increasing the height h [20] similar to our figure 2b of rope coiling. The rope deviates transversely from its axis with the farthest distance in the coiling region. This farthest transverse displacement sets the length scale for the coiling radius R. However, in the vicinity of the feeding point the rope hangs vertically straight with no transverse displacement. A family of curves satisfy the two-point boundary conditions at the point of contact, eq. (9), and at the feeding point, eq. (10). There exist many possible shapes which the rope can assume. The shape of the rope varies from catenary-like for slow feeding velocity to helix-like for fast feeding velocity. The stronger inertial force, provided by the fast feeding velocity, introduces an extra curvature to the straight portion below the feeding point. The rope retains the curvature throughout its entire length, and will look like a helix. An increase in the feeding velocity v increases the persistence length λ_p, while an increase in the height h slightly alters λ_p.

The richer variant of rope coiling arises when the plane is allowed to move horizontally with constant velocity u, for example, feeding the rope from the height onto a moving conveyor belt. The movement of the conveyor belt breaks the rotational symmetry of the circular coiling. Unlike its static counterpart, the coiling is no longer circular and bifurcates to a large variety of patterns. As the velocity of the conveyor belt u increases from zero, the pattern left on the conveyor belt varies subsequently from the translated coiling, alternating loops, meandering, and eventually to straight line [21]. The parameter which mainly controls the pattern formation is a mismatch between the feeding velocity v and the velocity of the conveyor belt u. A series of these patterns also appears if the the rope is replaced by a highly viscous liquid [22]. Only the differences between the rope patterns and the liquid patterns on a conveyor belt are two-fold, the length scale of pattern and the critical velocity of conveyor belt u_c at which the new pattern emerges. The resemblance between rope coiling and liquid rope coiling in the static case, $u = 0$, extends to the dynamical case, $u \neq 0$. This similarity that exists both in static case and in dynamical case suggests that the rope and the highly viscous liquid surprisingly belong to the same class of soft matters [23], despite the former being solid and the latter being liquid.

Acknowledgements

The author is grateful to M Fuangfoong and C Pattamaprom for useful discussion. He is indebted to P Pharob and N Teerachtragoon for the machine-shop assistance, and to P Srinukool for the measurement of the Young's modulus. He also gratefully acknowledges an anonymous reviewer for the constructive comments and invaluable suggestions. This work has been supported by the DPST-graduate start-up research grant, contract number 24/2557, and by the TU new research scholar, contract number 4/2557.

References

[1] A A Travers and J M T Thompson, *Phil. Trans. R. Soc. Lond. A* **362**, 1265 (2004)
[2] A R Singh, D Giri and S Kumar, *Pramana – J. Phys.* **71**, 283 (2008)
[3] C W Wolgemuth, T R Powers and R E Goldstein, *Phys. Rev. Lett.* **84**, 1623 (2000)
[4] M A Dias, L H Dudte, L Mahadevan and C D Santangelo, *Phys. Rev. Lett.* **109**, 114301 (2012)
[5] Y Kantor, *Pramana – J. Phys.* **64**, 1011 (2005)
[6] D M Raymer and D E Smith, *Proc. Natl. Acad. Sci.* **104**, 16432 (2007)
[7] E Bayart, S Deboeuf, F Corson, A Boudaoud and M A Bedia, *Europhys. Lett.* **95**, 34002 (2011)
[8] J L Silverberg, R D Noar, M S Packer, M J Harrison, C L Henley, I Cohen and S J Gerbode, *Proc. Natl. Acad. Sci.* **109**, 16794 (2012)
[9] A C Callan-Jones, P T Brun and B Audoly, *Phys. Rev. Lett.* **108**, 174302 (2012)
[10] L Mahadevan and J B Keller, *SIAM Rev.* **41**, 115 (1999)
[11] E Cerda and L Mahadevan, *Phys. Rev. Lett.* **90**, 74302 (2003)
[12] H King, R D Schroll, B Davidovitch and N Menon, *Proc. Natl. Acad. Sci.* **109**, 9716 (2012)
[13] N M Ribe, M Habibi and D Bonn, *Annu. Rev. Fluid Mech.* **44**, 249 (2012)
[14] M Pineirua, M A Bedia and S Moulinet, *Europhys. Lett.* **104**, 14005 (2013)
[15] M Habibi, N M Ribe and D Bonn, *Phys. Rev. Lett.* **99**, 154302 (2007)
[16] M K Jawed and P M Reis, *Extreme Mech. Lett.* **1**, 76 (2014)
[17] L Mahadevan and J B Keller, *Proc. R. Soc. Lond. A* **452**, 1679 (1996)
[18] S S Antman, *Nonlinear problems of elasticity* (Springer, Berlin, 2005)
[19] L D Landau and E M Lifshitz, *Theory of elasticity* (Pergamon, Oxford, 1970)

[20] N M Ribe, *Proc. R. Soc. Lond. A* **460**, 3223 (2004)
[21] M K Jawed, F Da, J Joo, E Grinspun and P M Reis, *Proc. Natl. Acad. Sci.* **111**, 14663 (2014)
[22] S W Morris, J H P Dawes, N M Ribe and J R Lister, *Phys. Rev. E* **77**, 66218 (2008)
[23] R Bandyopadhyay, *Pramana – J. Phys.* **81**, 3 (2013)